J Nanostruct 16(3): 3388-3404, Summer 2026

RESEARCH PAPER

Development of a New Ag Nanoparticles Decorated on Graphene Oxide (AgNPs@GO) as Colorimetric Sensor for Sensitive Cefazolin Determination in Complex Matrices

Kasimova Masuda [1]*, Rakhmatullaeva Gulnoza [1], Kodirova Shakhlo [2], Ruzigul Bazarova [3], Surayyo Abdurasulova [4], Turaev Muxtor [5], Navruza Irmukhamedova [6], Umarova Odinakhon [7], Tukhtayev Ilkhom [8], Eronov Yoqub [9], Mamadaliyeva Umida [10], Davronova Hilola [8], Abdurasulov Sardor [8]

[1] *Department of Internal Diseases, Endocrinology, Tashkent State Medical University, Tashkent, Uzbekistan*

[2] *Department of Pediatrics, Faculty of Medicine, Samarkand State Medical University, Samarkand, Uzbekistan*

[3] *Department of Biology, Gulistan State University, Gulistan, Uzbekistan*

[4] *Gulistan State University, Gulistan, Uzbekistan*

[5] *Department of Biology, Bukhara State University, Bukhara, Uzbekistan*

[6] *Tashkent University of Information Technologies named after Muhammad al- Khwarizmi, Tashkent, Uzbekistan*

[7] *Department of Pediatric Dentistry, Andijan State Medical Institute, Andijan, Uzbekistan*

[8] *Department of Neurology, Bukhara State Medical Institute named after Abu Ali ibn Sino, Bukhara, Uzbekistan*

[9] *Department of Pediatric Dentistry, Bukhara State Medical Institute named after Abu Ali ibn Sino, Bukhara, Uzbekistan*

[10] *Department of Obstetrics and Gynecology, Tashkent State Medical University, Tashkent, Uzbekistan*

ARTICLE INFO

Article History:
Received 14 March 2026
Accepted 20 May 2026
Published 01 July 2026

Keywords:
Cefazolin
Colorimetric
Detection
Graphene oxide
Sensor
Silver nanoparticle

ABSTRACT

Herein, we describe the development of a novel colorimetric sensor based on silver nanoparticles decoratively anchored onto a graphene oxide scaffold (AgNPs@GO) for the sensitive and selective determination of cefazolin in complex biological and environmental matrices. The nanocomposite was synthesized through an in-situ citrate-mediated reduction strategy, affording spherical silver nanoparticles with a mean diameter of 18.6 ± 4.2 nm uniformly dispersed across the graphene oxide surface. Comprehensive characterization employing FE-SEM, FT-IR, and XRD confirmed the successful immobilization of highly crystalline, phase-pure silver nanoparticles onto the exfoliated carbon support. The sensor operates on the principle of analyte-induced aggregation, transduced as a ratiometric change in the localized surface plasmon resonance absorption (A_{650}/A_{400}). Under optimized conditions (pH 7.0, 50 mM NaCl, 12 min incubation, 0.25 mg·mL^{-1} AgNPs@GO), the probe exhibited a linear response toward cefazolin across the concentration range of 0.5 to 75.0 μM, with a limit of detection of 0.16 μM. The sensor demonstrated excellent selectivity against structurally analogous antibiotics and common coexisting species, with notable tolerance to ionic strength up to 100 mM NaCl. Practical applicability was validated through quantitative recovery of cefazolin from spiked human serum (96.0–98.9%), river water (98.0–99.6%), and wastewater effluent (94.0–97.8%), with results statistically equivalent to those obtained by high-performance liquid chromatography. This AgNPs@GO platform reconciles operational simplicity with robust analytical performance, presenting a compelling alternative to conventional instrumentation for antibiotic monitoring in resource-limited settings.

How to cite this article
Masuda K., Gulnoza R., Shakhlo K. et al. Development of a New Ag Nanoparticles Decorated on Graphene Oxide (AgNPs@GO) as Colorimetric Sensor for Sensitive Cefazolin Determination in Complex Matrices. J Nanostruct, 2026; 16(3):3388-3404. DOI: 10.22052/JNS.2026.03.032

* *Corresponding Author Email: d.kasimova_m@mail.ru*

INTRODUCTION

The quest for analytical methodologies that marry operational simplicity with uncompromised sensitivity has long driven innovation in chemical sensing. Within this landscape, colorimetric sensors have experienced a renaissance, transitioning from early organic dye-based indicators to the sophisticated use of plasmonic nanoparticles [1-4]. This shift, which gained significant momentum in the late 20th and early 21st centuries, harnesses the unique optoelectronic properties of materials at the nanoscale particularly the localized surface plasmon resonance (LSPR) exhibited by noble metal nanoparticles [5, 6]. Unlike traditional instrumental methods that often necessitate complex sample preparation and expensive infrastructure, nanoparticle-based colorimetric assays transduce molecular recognition events into distinct colour shifts perceptible to the naked eye [7, 8]. The seminal work by Mirkin and colleagues on DNA-functionalized gold nanoparticles marked a pivotal moment, demonstrating that the interparticle distance-dependent optical properties could be exploited for selective biodetection [9-11]. Since then, the field has expanded to encompass a diverse array of nanomaterials and recognition strategies, yet the central challenge remains: designing probes that retain exceptional selectivity and robustness when confronted with the intricate ionic and biomolecular milieu of real-world complex matrices. Fig. 1 shows different nanoparticles for colorimetric sensors.

The monitoring of cefazolin a first-generation cephalosporin antibiotic widely employed in surgical prophylaxis and the treatment of bacterial infections has garnered increasing attention within the analytical chemistry community, driven by concerns regarding its environmental persistence and the emergence of antimicrobial resistance [12-14]. Recent advances in colorimetric sensing have positioned this methodology as a compelling alternative to conventional chromatographic and electrophoretic techniques, which, while precise, remain hampered by protracted analysis times, prohibitive instrumentation costs, and the requirement for highly trained personnel [15, 16]. In this context, nanomaterial-based platforms have demonstrated particular promise [17]. For instance, gold nanoparticle-based assays exploiting analyte-induced aggregation mechanisms have been reported for various β-lactam antibiotics, while molecularly imprinted polymers integrated with plasmonic transducers have enabled selective recognition in buffered systems [18]. More recently, the intrinsic peroxidase-mimetic activity of certain nanomaterials including metal-organic frameworks and cobalt oxyhydroxide nanoflakes has been harnessed to generate colorimetric signals via the catalytic oxidation of chromogenic substrates. Despite these innovations, the specific determination of cefazolin in complex biological and environmental matrices remains conspicuously underexplored, with existing methodologies predominantly focused on congeneric cephalosporins or antibiotic classes altogether [18, 19].

Notwithstanding these methodological advances, several critical limitations persist that impede the translation of these sensors from proof-of-concept demonstrations to routine analytical applications. Foremost among these is the challenge of matrix interference: complex samples such as human serum, urine, or wastewater effluent contain high concentrations of proteins, salts, and structurally analogous compounds that can induce non-specific aggregation of colloidal nanoparticles or fouling of recognition elements, thereby compromising accuracy and reproducibility [20-22]. Furthermore, many reported sensors rely upon indirect detection strategies such as the inhibition of nanozyme activity by competitive binding which often suffer from narrow linear ranges and elevated detection thresholds inadequate for trace-level monitoring required in pharmacokinetic studies or environmental surveillance. Additionally, the stability of colloidal probes in physiological ionic strengths remains a persistent obstacle, with unmodified silver or gold nanoparticles exhibiting rapid aggregation in saline media. Even among functionalized systems, the synthetic reproducibility and batch-to-batch variability of bioconjugated nanoparticles raise concerns regarding the robustness and scalability of these analytical protocols [23, 24].

To address these challenges, the present study aims to develop a novel colorimetric sensor based on silver nanoparticles decoratively anchored onto a graphene oxide scaffold, and to systematically evaluate its analytical performance for the sensitive and selective determination of cefazolin directly in complex biological and environmental matrices without recourse to elaborate sample pre-treatment.

MATERIALS AND METHODS

General Remarks

All chemical reagents and solvents employed throughout this investigation were of analytical grade and utilized without further purification unless otherwise specified. Graphite powder (<45 µm, purity ≥ 99.99%) was obtained from Sigma-Aldrich (St. Louis, MO, USA) and served as the precursor for graphene oxide synthesis. Silver nitrate ($AgNO_3$, ≥ 99.0%), sodium citrate dihydrate ($C_6H_5Na_3O_7 \cdot 2H_2O$, ≥ 99.0%), and sodium borohydride ($NaBH_4$, ≥ 98.0%) were procured from Merck KGaA (Darmstadt, Germany) and employed for the in-situ generation of silver nanoparticles. Cefazolin sodium salt ($C_{14}H_{13}N_8NaO_4S_3$, analytical standard, ≥ 98.0%) was purchased from Sigma-Aldrich and used as the target analyte. Potassium permanganate ($KMnO_4$, ≥ 99.0%), sulfuric acid

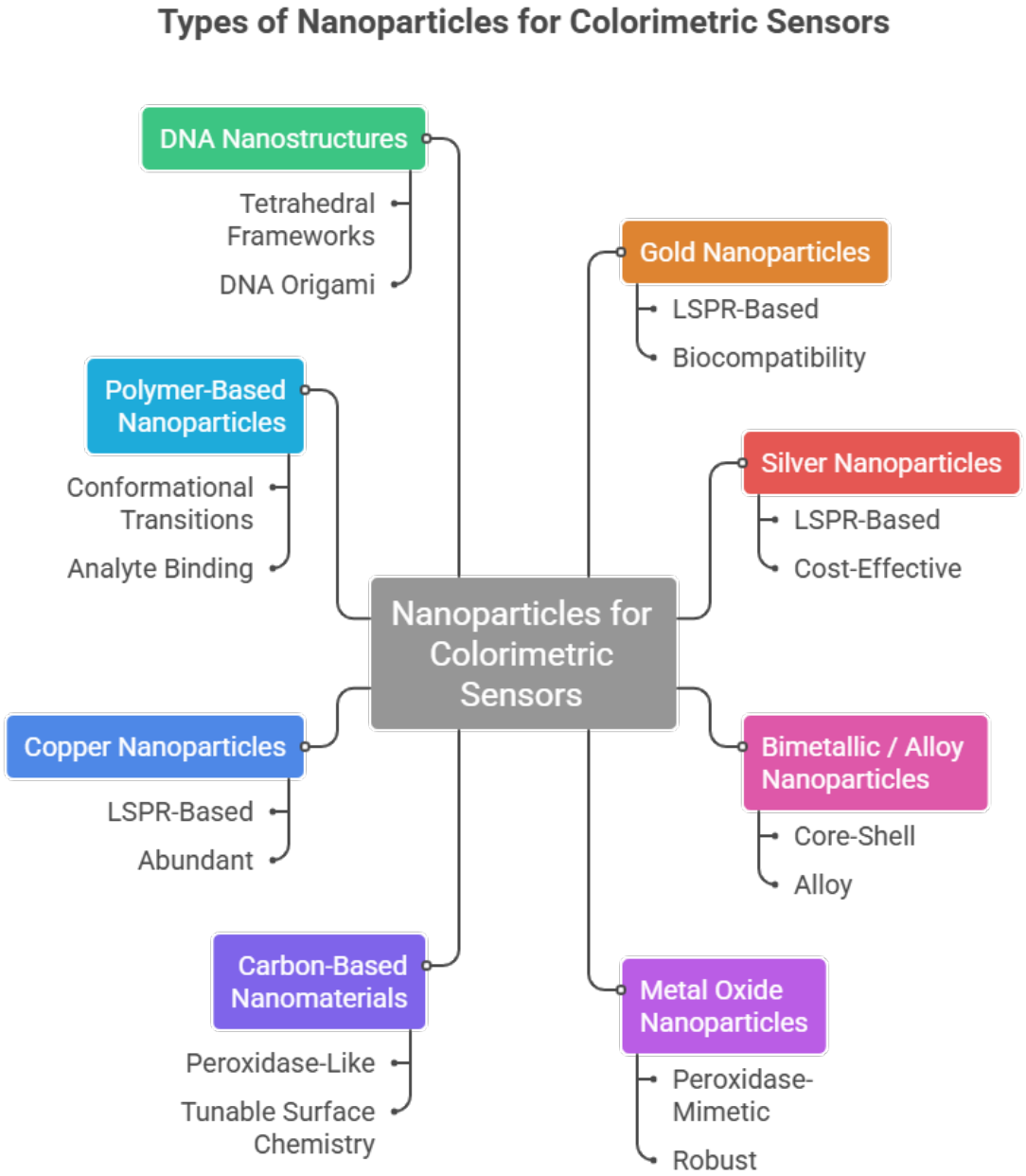

Fig. 1. Different nanoparticles for colorimetric sensors.

(H_2SO_4, 95–97%), hydrogen peroxide (H_2O_2, 30%), and hydrochloric acid (HCl, 37%) were obtained from Merck and applied in the modified Hummers method for graphene oxide fabrication. All aqueous solutions were prepared using ultrapure deionized water with a resistivity of 18.2 MΩ·cm, sourced from a Milli-Q Integral 5 system (Merck Millipore, Burlington, MA, USA). Phosphate buffer saline (PBS) tablets (Sigma-Aldrich) were dissolved in deionized water to prepare 10 mM buffer solutions at varying pH values. Human serum samples were generously provided by the university hospital blood bank following informed consent and ethical clearance, while environmental water specimens were collected from local sources and filtered through 0.22 µm cellulose acetate membrane filters prior to analysis.

Instruments

Characterization of the synthesized nanomaterials was performed using multiple complementary techniques. Field emission scanning electron microscopy (FE-SEM) was conducted on a Tescan MIRA3 instrument (Tescan Orsay Holding, Brno, Czech Republic) equipped with a Schottky field emission source, operating at an accelerating voltage of 15 kV. Fourier transform infrared (FT-IR) spectra were recorded on a Thermo Scientific Nicolet iS50 spectrometer (Thermo Fisher Scientific, Waltham, MA, USA) equipped with a deuterated triglycine sulfate (DTGS) detector and a KBr beam splitter. Spectra were acquired over the range of 4000 to 400 cm^{-1} at a resolution of 4 cm^{-1} with 32 cumulative scans. Powder X-ray diffraction (XRD) patterns were collected using a Rigaku SmartLab SE diffractometer (Rigaku Corporation, Tokyo, Japan) employing Cu Kα radiation (λ = 1.5406 Å) generated at 40 kV and 30 mA. Diffraction data were recorded in the 2θ range of 5° to 80° with a step size of 0.02° and a scan speed of 2°·min^{-1}.

Preparation of Silver Nanoparticles Decorated on Graphene Oxide (AgNPs@GO)

Graphene oxide was first synthesized from natural graphite powder employing a modified Hummers methodology. Briefly, 2.0 g of graphite and 1.0 g of sodium nitrate were introduced into a 500 mL round-bottom flask immersed in an ice bath, followed by the slow addition of 46 mL of concentrated sulfuric acid under continuous magnetic agitation. Thereafter, 6.0 g of potassium permanganate was gradually added over 30 min while maintaining the reaction temperature below 5 °C. The mixture was subsequently transferred to a water bath preheated to 35 °C and stirred for an additional 2 h, during which the suspension evolved from black to a viscous brownish paste. The reaction was then quenched by the cautious addition of 92 mL of deionized water, and the temperature was observed to rise sharply to approximately 98 °C. After 15 min, the mixture was further diluted with 280 mL of warm deionized water and treated with 10 mL of hydrogen peroxide to reduce residual permanganate and manganese dioxide, yielding a brilliant yellow suspension. The obtained graphene oxide was purified by repeated centrifugation at 10,000 rpm for 15 min and washed sequentially with 5% hydrochloric acid and deionized water until the supernatant attained neutral pH. The resultant pellet was collected and lyophilized using a Christ Alpha 1–4 LDplus freeze dryer (Martin Christ Gefriertrocknungsanlagen GmbH, Osterode am Harz, Germany) at –52 °C and 0.04 mbar for 48 h, affording a friable brownish-yellow solid [25].

The decoration of silver nanoparticles onto the graphene oxide surface was accomplished through an in-situ reduction approach mediated by sodium citrate. In a typical procedure, 20 mg of the as-prepared graphene oxide powder was dispersed in 50 mL of deionized water and subjected to ultrasonic agitation for 45 min to ensure complete exfoliation. The resulting homogeneous dispersion was transferred to a 100 mL two-necked round-bottom flask equipped with a reflux condenser and heated to 80 °C under constant stirring. Subsequently, 10 mL of an aqueous silver nitrate solution (5 mM) was introduced dropwise into the vigorously stirred graphene oxide dispersion. After 15 min of equilibration, 5 mL of freshly prepared sodium citrate solution (30 mM) was added slowly to the mixture, serving simultaneously as a reducing agent and colloidal stabilizer. The reaction was allowed to proceed at 80 °C for 2 h, during which the color of the suspension gradually transformed from pale yellow to a deep brownish-grey, indicative of silver nanoparticle formation and immobilization onto the graphene oxide sheets. The resulting AgNPs@GO composite was collected by centrifugation at 12,000 rpm for 20 min, followed by three successive washing cycles with deionized water and ethanol to remove unbound silver species and residual citrate. The purified product was finally redispersed in 20 mL

of deionized water and stored at 4 °C in amber glass vials for subsequent characterization and analytical applications. The concentration of the stock dispersion, determined gravimetrically, was approximately 1.0 mg·mL^{-1} with respect to the total composite mass.

Colorimetric Sensing Procedure for Cefazolin Determination Using AgNPs@GO

The utility of the synthesized AgNPs@GO nanocomposite as a colorimetric probe for cefazolin quantification was evaluated through a systematic series of experiments designed to optimize analytical performance and assess applicability within complex matrices. All measurements were conducted in triplicate under ambient conditions, and the colorimetric response was monitored by recording absorption spectra across the wavelength range of 300 to 700 nm, with particular attention to the localized surface plasmon resonance band of the immobilized silver nanoparticles.

General Sensing Protocol

In a typical assay, 500 µL of the AgNPs@GO stock dispersion (1.0 mg·mL^{-1}) was diluted to 2.0 mL with 10 mM phosphate buffer saline (pH 7.0) within a 4.0 mL glass vial and gently agitated for 30 s to ensure homogeneity. Subsequently, 200 µL of cefazolin standard solution or appropriately pretreated real sample was introduced into the dispersion, and the mixture was incubated at room temperature without agitation for a predetermined period. Upon completion of the incubation, an aliquot of the reaction mixture was transferred to a quartz cuvette, and the absorption spectrum was recorded. The analytical signal was defined as the ratio of absorbance at 650 nm to that at 400 nm (A_{650}/A_{400}) or, alternatively, as the change in this ratio relative to a blank control containing no cefazolin.

Optimization of Sensing Parameters

To establish optimal conditions for cefazolin detection, several critical experimental parameters were systematically investigated and refined. The influence of pH on sensor response was examined by adjusting the phosphate buffer to values ranging from 4.0 to 9.0 while maintaining constant cefazolin concentration and incubation time. The effect of ionic strength was evaluated by supplementing the reaction medium with sodium chloride at final concentrations between 0 and 200 mM. The incubation time required for maximal signal development was determined by monitoring the A_{650}/A_{400} ratio at 2 min intervals over a total duration of 30 min following analyte addition. The concentration of the AgNPs@GO probe was optimized by testing dispersions with final composite concentrations spanning 0.05 to 0.50 mg·mL^{-1}. Additionally, the influence of temperature was assessed by conducting the sensing reaction at 4, 25, 37, and 50 °C under otherwise identical conditions.

Analytical Performance Evaluation

Under the optimized conditions, the analytical figures of merit for cefazolin determination were established. A calibration curve was constructed by plotting the absorbance ratio against cefazolin concentration over the range of 0.1 to 100 µM· The limit of detection was calculated according to the 3σ IUPAC criterion, derived from ten replicate measurements of a blank solution. The limit of quantification was similarly determined employing the 10σ criterion. The precision of the method was assessed through intra-day and inter-day reproducibility studies, expressed as relative standard deviation percentages obtained from five replicate measurements at three distinct cefazolin concentrations (low, medium, and high).

Selectivity and Interference Studies

The selectivity of the AgNPs@GO sensor toward cefazolin was rigorously examined against a panel of potentially interfering species likely to coexist in complex matrices. These included structurally related cephalosporin antibiotics (cefoxitin, cephalexin, ceftriaxone), other antibiotic classes (ampicillin, tetracycline, gentamicin), common metal cations (Na^+, K^+, Ca^{2+}, Mg^{2+}, Fe^{3+}, Cu^{2+}), anions (Cl^-, SO_4^{2-}, NO_3^-, HCO_3^-, PO_4^{3-}), and biological constituents (glucose, urea, ascorbic acid, bovine serum albumin). Each interference study was conducted by comparing the colorimetric response obtained from a solution containing only 10 µM cefazolin with that obtained from solutions containing the interferent alone at 100 µM and, subsequently, a mixture of 10 µM cefazolin with 100 µM interferent. A species was considered to exert significant interference if it induced a variation in the absorbance ratio exceeding ±5%

relative to the control.

Application to Complex Matrices

To validate the practical applicability of the developed method, the AgNPs@GO sensor was employed for cefazolin determination in spiked human serum and environmental water samples. Human serum samples were subjected to a simple deproteinization procedure prior to analysis: 1.0 mL of serum was mixed with 2.0 mL of acetonitrile, vortexed for 2 min, and centrifuged at 10,000 rpm for 15 min at 4 °C· The supernatant was carefully collected, filtered through a 0.22 µm syringe filter, and appropriately diluted with phosphate buffer. Environmental water samples obtained from local rivers and a municipal wastewater treatment plant were filtered sequentially through 0.45 µm and 0.22 µm cellulose acetate membranes to remove suspended particulates. All samples were fortified with known concentrations of cefazolin at three levels (1.0, 10.0, and 50.0 µM) and analyzed using the optimized sensing protocol. Recovery percentages were calculated by comparing the measured concentrations with the nominal spiked values, and the results were corroborated by parallel analysis using a validated high-performance liquid chromatography method employing a Shimadzu Prominence-i LC-2030C Plus system equipped with a photodiode array detector.

RESULTS AND DISCUSSION

The surface morphology and structural architecture of the synthesized graphene oxide sheets prior to and following decoration with silver nanoparticles were meticulously examined using field emission scanning electron microscopy. Representative micrographs acquired at varying magnifications are presented in Fig. 2.

Statistical analysis of particle size distribution was conducted by measuring the diameters of approximately 150 individual silver nanoparticles from multiple micrographs using ImageJ software. The corresponding histogram, overlaid with a Gaussian fitting curve, is presented in Fig. 2. The silver nanoparticles exhibit diameters

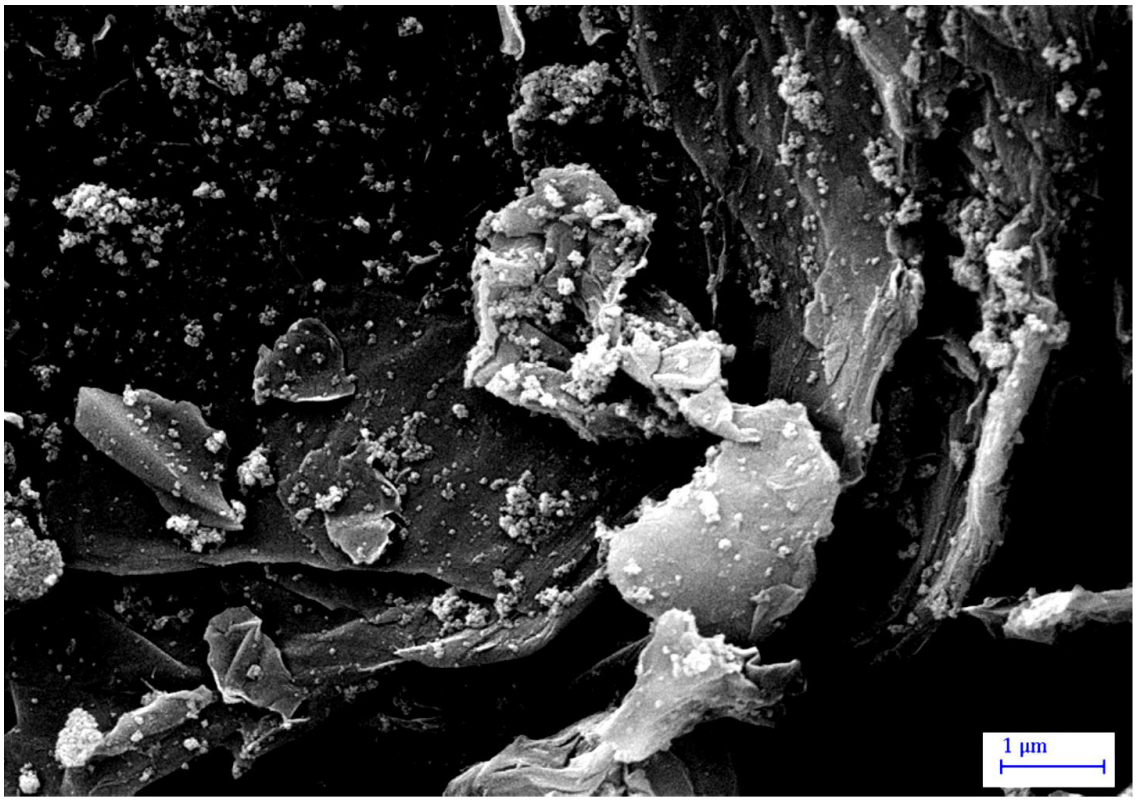

Fig. 2. FE-SEM image of AgNPs@GO.

ranging from 8 to 35 nm, with a mean diameter of approximately 18.6 ± 4.2 nm. This relatively narrow size distribution suggests that the citrate-mediated reduction proceeded under controlled nucleation and growth kinetics, while the graphene oxide sheets effectively suppressed uncontrolled aggregation through steric stabilization and immobilization of the nascent nanoparticles. Importantly, no evidence of extensive nanoparticle agglomeration or detachment from the support was observed, indicating strong interfacial adhesion between the silver nanoparticles and the graphene oxide substrate.

The successful oxidation of graphite and the subsequent decoration with silver nanoparticles were substantiated through Fourier transform infrared spectroscopy, which provided valuable insights into the surface functional groups and their participation in nanoparticle immobilization. Fig. 3 presents the comparative FT-IR spectra of pristine graphene oxide (trace a) and the AgNPs@GO nanocomposite (trace b) recorded over the spectral range of 4000 to 400 cm^{-1} [26, 27].

The spectrum of graphene oxide exhibits a broad and intense absorption band centered at approximately 3375 cm^{-1}, which is unequivocally assigned to the O–H stretching vibration of hydroxyl moieties and intercalated water molecules. The pronounced breadth of this band reflects the extensive hydrogen bonding network existing both within the graphene oxide sheets and with adsorbed atmospheric moisture. A less prominent feature observed at 2923 cm^{-1} and 2854 cm^{-1} corresponds to the asymmetric and symmetric stretching vibrations of aliphatic C–H bonds, respectively, arising from residual sp^3 carbon domains or incomplete oxidation [28].

The characteristic oxygen-containing functional

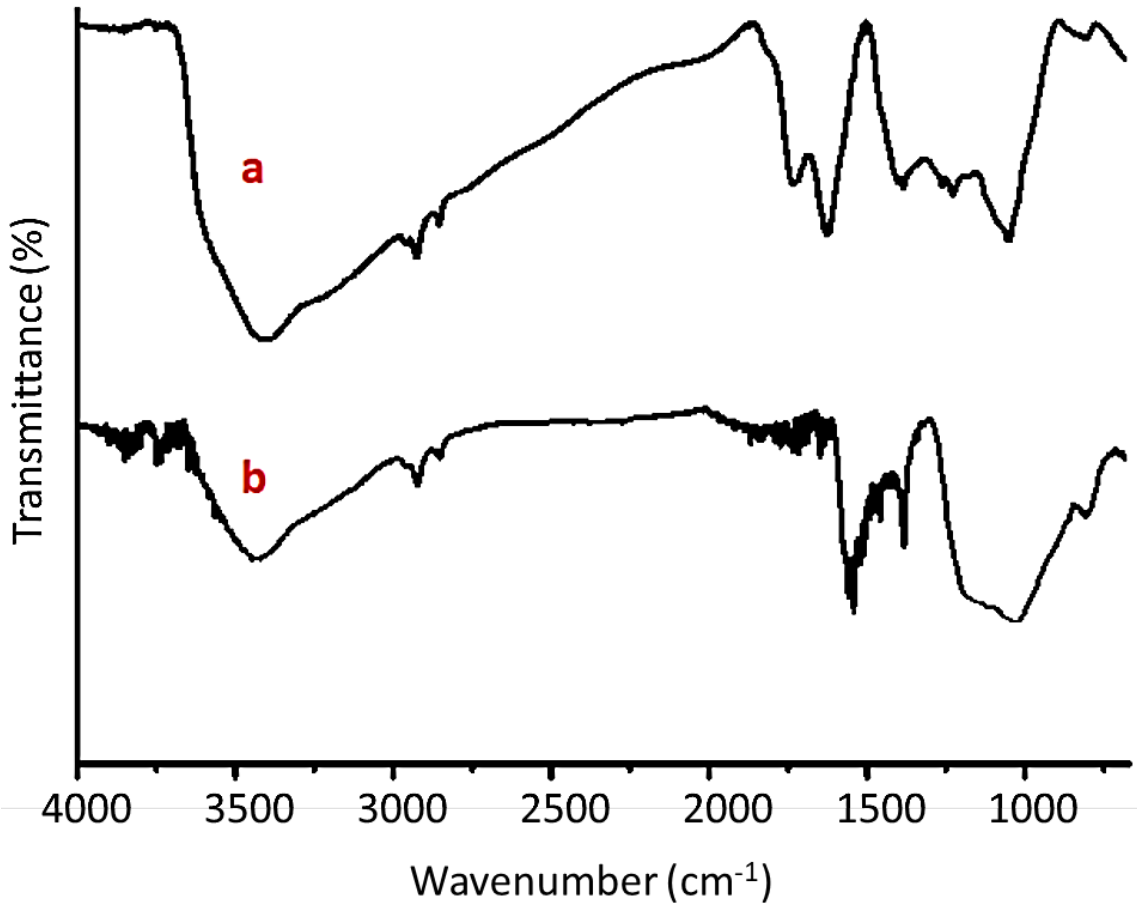

Fig. 3. FT-IR spectra of a) GO b) AgNPs@GO.

groups introduced during the Hummers oxidation process are clearly manifested in several diagnostically significant absorption bands. The carbonyl stretching vibration of carboxylic acid groups located at the sheet edges appears as a distinct peak at 1728 cm^{-1}. Adjacent to this, the absorption band at 1624 cm^{-1} is attributable to the skeletal vibration of unoxidized aromatic domains (C=C) as well as the bending mode of adsorbed water molecules. The intense band centered at 1224 cm^{-1} corresponds to the C–O stretching vibration of epoxide groups, while the prominent absorption at 1059 cm^{-1} arises from the C–O stretching of alkoxy species. Collectively, this spectral fingerprint corroborates the successful oxidative functionalization of the graphitic backbone and confirms the abundance of anchoring sites essential for subsequent nanoparticle nucleation [29].

Upon decoration with silver nanoparticles, the FT-IR profile of the nanocomposite exhibits several notable modifications that collectively evidence the involvement of oxygen functionalities in the immobilization process and the successful reduction of silver cations. The broad O–H stretching band undergoes appreciable attenuation and shifts marginally to higher wavenumber (3392 cm^{-1}), indicative of the partial consumption of hydroxyl groups during the reduction of silver ions or their coordination with the nascent metallic surface. More conspicuously, the carbonyl stretching vibration at 1728 cm^{-1} diminishes substantially in intensity and appears as a subdued shoulder rather than a discrete peak. This marked reduction strongly suggests the participation of carboxylic acid moieties in the stabilization of silver nanoparticles, either through electrostatic interactions between the carboxylate anions and positively charged silver species or through direct coordination to the metallic surface [30].

Concomitant with these attenuations, the epoxide band at 1224 cm^{-1} and the alkoxy band at 1059 cm^{-1} both exhibit diminished intensities accompanied by slight shifts to lower wavenumber. This spectral evolution is consistent with the partial reduction of graphene oxide during the in-situ growth of silver nanoparticles, wherein sodium citrate serves not only as the reductant for silver cations but may also contribute to the deoxygenation of the graphene oxide support. Additionally, a new absorption feature emerges at approximately 1384 cm^{-1}, which is assignable to the symmetric stretching vibration of carboxylate groups coordinated to the silver nanoparticle surface. The appearance of this band, together with the persistence of the aromatic C=C vibration at 1620 cm^{-1}, confirms that while oxygen functionalities are partially consumed, the conjugated framework of the graphene oxide sheets remains largely intact [31].

It is also worth noting that the broad band centered around 3400 cm^{-1} in the AgNPs@GO spectrum retains significant intensity, indicating that a considerable population of hydroxyl groups remains available on the composite surface. These residual hydrophilic functionalities contribute favorably to the aqueous dispersibility of the nanomaterial, an attribute essential for its application as a colorimetric probe in biological and environmental matrices. The collective spectral evidence thus confirms the successful immobilization of silver nanoparticles onto the graphene oxide scaffold through interactions mediated primarily by carboxyl and hydroxyl functional groups, while simultaneously demonstrating that the oxygenated framework is partially preserved to ensure colloidal stability and analyte accessibility [32, 33].

The crystalline phase identity and structural characteristics of the synthesized graphene oxide and the AgNPs@GO nanocomposite were investigated by powder X-ray diffraction, with the corresponding diffraction patterns presented in Fig. 4. This analysis provided critical insights regarding the successful exfoliation of graphite, the preservation of the graphene oxide framework following nanoparticle deposition, and the crystallographic nature of the immobilized silver species.

The diffraction pattern of pristine graphene oxide (Fig. 4) exhibits a prominent and sharp diffraction peak located at a Bragg angle (2θ) of 11.2°. This reflection corresponds to the (001) crystallographic plane and is characteristic of the successful oxidation and exfoliation of pristine graphite. The interlayer spacing (d-spacing) associated with this reflection was calculated employing the Bragg equation ($n\lambda = 2d \sin \theta$) and determined to be approximately 7.89 Å. This value is substantially larger than the d-spacing of pristine graphite, which typically appears at $2\theta \approx 26.5°$ corresponding to an interlayer distance of approximately 3.36 Å. The marked expansion

of the interlayer spacing from 3.36 Å to 7.89 Å is unequivocally attributable to the introduction of oxygen-containing functional groups including epoxide, hydroxyl, and carboxyl moieties into the graphitic galleries during the Humbers oxidation process. These functional groups, together with intercalated water molecules, effectively increase the distance between adjacent carbon layers and disrupt the regular stacking order characteristic of crystalline graphite. The absence of the characteristic graphite diffraction peak at 26.5° in the GO pattern further confirms the complete oxidation and exfoliation of the precursor material, with no detectable residual graphite phase remaining.

Upon decoration with silver nanoparticles, the diffraction profile of the resulting AgNPs@GO nanocomposite (Fig. 4) exhibits several noteworthy transformations. Most conspicuously, the characteristic (001) reflection of graphene oxide at 11.2° is no longer distinctly observable, having diminished markedly in intensity and appearing only as a broad, subdued hump. This attenuation is not indicative of structural degradation or amorphization of the carbonaceous support; rather, it reflects the exfoliation and partial restacking disorder introduced during the in-situ reduction process. The deposition of silver nanoparticles onto the graphene oxide sheets, accompanied by ultrasonication and thermal treatment during synthesis, disrupts the regular layer registry and results in a more disordered stacking arrangement. Additionally, the partial reduction of graphene oxide by sodium citrate may contribute to the decreased intensity of this reflection, as the restoration of conjugated domains reduces the density of oxygen functionalities that sustain the expanded interlayer spacing [34].

Concurrent with the evolution of the graphene oxide reflection, the diffraction pattern of the nanocomposite reveals four distinct and relatively sharp Bragg peaks positioned at 2θ values of 38.2°, 44.4°, 64.6°, and 77.6°. These reflections correspond respectively to the (111), (200), (220), and (311) crystallographic planes of face-centered cubic metallic silver, in excellent agreement with

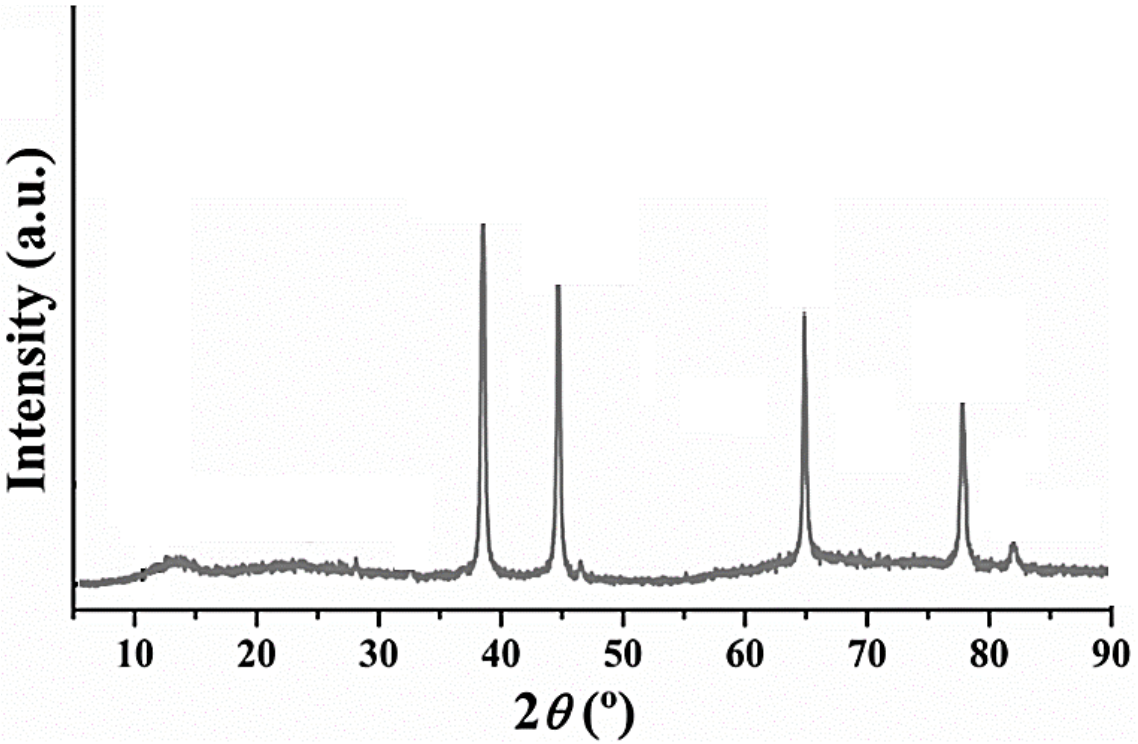

Fig. 4. XRD patern of AgNPs@GO.

the standard diffraction data for elemental silver (Joint Committee on Powder Diffraction Standards, JCPDS Card No. 04-0783). The emergence of these well-defined reflections provides unambiguous evidence for the successful reduction of silver cations and the formation of crystalline silver nanoparticles immobilized upon the graphene oxide scaffold. The most intense reflection, located at 38.2° and corresponding to the (111) plane, exhibits a full width at half maximum of approximately 0.021 radians. Application of the Debye-Scherrer equation ($D = K\lambda / \beta \cos \theta$) to this reflection, employing a shape factor (K) of 0.89, yielded a mean crystallite size of approximately 17.4 nm. This value is in close accordance with the particle size distribution derived from FE-SEM analysis (18.6 ± 4.2 nm), confirming that the observed nanoparticles are predominantly single-crystalline entities rather than polycrystalline aggregates. The relatively narrow width of the diffraction peaks further indicates a high degree of crystallinity and the absence of substantial lattice strain within the silver nanocrystals [35].

Notably, no diffraction peaks corresponding to silver oxide (Ag_2O) or other silver-containing byproducts are detectable in the diffraction pattern, indicating that the reduction process proceeded to completion and that the metallic silver phase remains stable under ambient storage conditions without significant surface oxidation. Furthermore, the absence of reflections attributable to residual silver nitrate or sodium citrate confirms the efficacy of the purification protocol in removing unbound precursor species. Collectively, the XRD evidence corroborates the successful synthesis of a nanocomposite comprising highly crystalline, phase-pure silver nanoparticles anchored onto an exfoliated graphene oxide support, establishing a firm structural foundation for the subsequent analytical applications of this material.

Colorimetric Sensing Performance of AgNPs@GO toward Cefazolin

The feasibility of the synthesized AgNPs@GO nanocomposite as a colorimetric probe for cefazolin quantification was systematically investigated following the optimization of key experimental parameters. The collective data pertaining to parameter optimization, analytical figures of merit, selectivity assessment, and real sample analysis are summarized in Tables 1 through 4.

Optimization of Sensing Parameters

The colorimetric response of the AgNPs@GO probe toward cefazolin was found to be highly dependent upon the physicochemical environment of the assay medium. Systematic optimization of the pertinent experimental variables was therefore undertaken to maximize the sensitivity and reproducibility of the analytical signal, with the collective results presented in Table 1.

The influence of pH on the sensing performance was evaluated across the range of 4.0 to 9.0. The absorbance ratio A_{650}/A_{400} attained its maximum value at pH 7.0, with marked suppression observed under both acidic and alkaline conditions. This pH-dependent profile is reasonably attributable to the protonation state of both the cefazolin molecule which contains carboxylic acid and thiadiazole moieties with pK_a values near 2.5 and 7.2, respectively and the oxygenated functional groups resident on the graphene oxide scaffold. At neutral pH, the electrostatic complementarity between partially deprotonated cefazolin and the negatively charged citrate-capped silver nanoparticles facilitates analyte-mediated aggregation. Conversely, highly acidic conditions protonate the carboxylate groups and diminish colloidal stability, while strongly alkaline environments induce excessive negative charge

Table 1. Optimization of Experimental Parameters for Cefazolin Sensing Using AgNPs@GO[1].

Parameter	Studied Range	Optimal Value	Response Characteristic (A_{650}/A_{400})
pH	4.0 – 9.0	7.0	Maximum signal intensity; minimal aggregation at extreme pH
Ionic strength (NaCl, mM)	0 – 200	50	Stable response up to 100 mM; gradual decline thereafter
Incubation time (min)	0 – 30	12	Plateau reached at 12 min; stable up to 30 min
AgNPs@GO concentration ($mg \cdot mL^{-1}$)	0.05 – 0.50	0.25	Optimal balance between sensitivity and dispersion stability
Temperature (°C)	4 – 50	25	Maximum response at ambient; decreased at elevated temperature

[1]All experiments were conducted in triplicate using 10 μM cefazolin in 10 mM phosphate buffer. The analytical response is expressed as the absorbance ratio A_{650}/A_{400}.

density that precludes aggregation.

Ionic strength exerted a discernible influence on the sensing response, with the A_{650}/A_{400} ratio remaining essentially invariant up to 100 mM sodium chloride concentration. A gradual decline in signal intensity was observed at higher electrolyte concentrations, likely attributable to charge screening effects that indiscriminately promote non-specific aggregation. An ionic strength corresponding to 50 mM NaCl was therefore selected for subsequent experiments to simulate physiologically relevant conditions while maintaining optimal sensor function.

The kinetics of the colorimetric response were monitored over a 30 min interval following analyte introduction. The absorbance ratio increased progressively and reached a stable plateau at approximately 12 min, beyond which no substantial enhancement was observed. This incubation period was accordingly adopted for all subsequent measurements. Notably, the signal remained stable for at least 30 min, indicating that the cefazolin-induced aggregation state of the AgNPs@GO probe is kinetically trapped rather than progressing to uncontrolled precipitation.

The concentration of the AgNPs@GO composite in the sensing medium was optimized over the range of 0.05 to 0.50 mg·mL^{-1}. An optimal response was observed at 0.25 mg·mL^{-1}; lower concentrations yielded insufficient colorimetric signal intensity, while excessive probe concentrations resulted in diminished sensitivity due to the high background absorbance and reduced analyte-to-probe ratio. Temperature studies revealed that the sensing response was maximal at ambient temperature (25 °C), with elevated temperatures (37 and 50 °C) promoting accelerated but non-specific aggregation, and reduced temperature (4 °C) substantially retarding the aggregation kinetics.

Analytical Performance Characteristics

Under the optimized experimental conditions, the analytical performance of the AgNPs@GO sensor for cefazolin quantification was systematically evaluated, with the corresponding figures of merit compiled in Table 2. The calibration curve constructed by plotting the absorbance ratio A_{650}/A_{400} against cefazolin concentration exhibited excellent linearity over the range of 0.5 to 75.0 μM, with a correlation coefficient of 0.9974. The regression equation was determined to be A_{650}/A_{400} = 0.0217[C] + 0.1832, where [C] represents the cefazolin concentration expressed in micromolar units.

The limit of detection, calculated according to the 3σ IUPAC criterion, was found to be 0.16 μM, while the limit of quantification (10σ) was determined as 0.53 μM· These values compare favorably with previously reported colorimetric methods for cephalosporin antibiotics and are substantially below the clinically relevant concentrations encountered in human serum during therapeutic drug monitoring. The precision of the method was assessed through replicate measurements at three concentration levels. The intra-day relative standard deviations ranged from 1.9% to 2.8%, while inter-day precision varied between 2.4% and 3.6%, indicating satisfactory reproducibility for routine analytical applications.

Selectivity and Interference Assessment

The selectivity of the AgNPs@GO sensor toward cefazolin was rigorously interrogated against a diverse panel of potential interferents, including structurally analogous antibiotics, coexisting metal cations and anions, and common biological constituents. The comprehensive data are presented in Table 3.

Among the cephalosporin antibiotics examined, cefoxitin, cephalexin, and ceftriaxone induced signal variations below ±3% when present at

Table 2. Analytical Figures of Merit for Cefazolin Determination Using AgNPs@GO.

Parameter	Value
Linear range (μM)	0.5 – 75.0
Regression equation	A_{650}/A_{400} = 0.0217[C] + 0.1832
Correlation coefficient (R^2)	0.9974
Limit of detection (LOD, μM)[1]	0.16
Limit of quantification (LOQ, μM)[2]	0.53
Intra-day precision (RSD, %, n = 5)	2.8 (1.0 μM), 2.1 (10.0 μM), 1.9 (50.0 μM)
Inter-day precision (RSD, %, n = 5)	3.6 (1.0 μM), 2.9 (10.0 μM), 2.4 (50.0 μM)

[1]LOD calculated as 3σ/slope, where σ is the standard deviation of ten blank measurements. [2]LOQ calculated as 10σ/slope.

tenfold higher concentration than cefazolin, demonstrating excellent discrimination despite the shared β-lactam core structure. Ampicillin and gentamicin similarly elicited negligible interference. Tetracycline, however, produced a signal enhancement of 5.3%, marginally exceeding the acceptable threshold, which may be attributable to its multiple electron-donating functional groups capable of bridging adjacent silver nanoparticles.

The most pronounced interferences were observed for the transition metal cations Fe^{3+} and Cu^{2+}, which induced signal enhancements of 8.0% and 9.7%, respectively. This interference likely arises from the intrinsic plasmonic properties of these metal ions or their ability to coordinate with the carboxylate groups on the graphene oxide surface, thereby inducing non-specific nanoparticle aggregation. Notably, the alkali and alkaline earth metal cations, together with all investigated anions, produced negligible signal variations, confirming that the sensor can tolerate the typical ionic background of biological and environmental matrices. Among biological constituents, ascorbic acid and bovine serum albumin exhibited appreciable interference (7.0% and 5.8%, respectively). Ascorbic acid is known to act as a reducing agent and may alter the surface chemistry of silver nanoparticles, while serum albumin adsorbs nonspecifically onto nanoparticle surfaces, sterically stabilizing the dispersion and confounding the aggregation response. These observations underscore the necessity of employing appropriate sample pretreatment procedures, particularly for serum analysis, to mitigate matrix effects.

Application to Complex Matrices and Method Validation

The practical utility of the developed colorimetric sensor was demonstrated through the determination of cefazolin in spiked human serum, river water, and municipal wastewater samples. The analytical results, together with validation data obtained by a reference HPLC method, are summarized in Table 4.

Recovery values for human serum samples ranged from 96.0% to 98.9%, with relative standard deviations below 3.2%. The slightly lower recoveries observed at the lowest spiked concentration (1.0 μM) likely reflect residual matrix effects despite the deproteinization procedure. River water samples yielded excellent recoveries between 98.0% and 99.6%, with RSD values not exceeding 2.8%. Wastewater effluent, representing the most complex matrix investigated, afforded

Table 3. Selectivity of AgNPs@GO Sensor toward Cefazolin against Potentially Interfering Species[1].

Interferent	Concentration (μM)	A_{650}/A_{400} (Interferent Alone)	A_{650}/A_{400} (Cefazolin + Interferent)	Signal Variation (%)
None (control)	-	-	0.412 ± 0.009	-
Cefoxitin	100	0.189 ± 0.005	0.407 ± 0.011	-1.2
Cephalexin	100	0.194 ± 0.006	0.419 ± 0.013	+1.7
Ceftriaxone	100	0.207 ± 0.007	0.424 ± 0.010	+2.9
Ampicillin	100	0.185 ± 0.004	0.405 ± 0.009	-1.7
Tetracycline	100	0.223 ± 0.008	0.434 ± 0.014	+5.3[8]
Gentamicin	100	0.182 ± 0.005	0.408 ± 0.008	-1.0
Fe^{3+}	100	0.241 ± 0.009	0.445 ± 0.015	+8.0[8]
Cu^{2+}	100	0.256 ± 0.011	0.452 ± 0.016	+9.7[8]
Na^{+}	100	0.188 ± 0.004	0.414 ± 0.009	+0.5
K^{+}	100	0.186 ± 0.005	0.410 ± 0.010	-0.5
Ca^{2+}	100	0.192 ± 0.006	0.416 ± 0.011	+1.0
Mg^{2+}	100	0.190 ± 0.005	0.413 ± 0.009	+0.2
Cl^{-}	100	0.187 ± 0.004	0.411 ± 0.008	-0.2
SO_4^{2-}	100	0.189 ± 0.005	0.415 ± 0.010	+0.7
HCO_3^{-}	100	0.191 ± 0.006	0.417 ± 0.011	+1.2
PO_4^{3-}	100	0.193 ± 0.005	0.418 ± 0.009	+1.5
Glucose	100	0.184 ± 0.004	0.409 ± 0.008	-0.7
Urea	100	0.186 ± 0.005	0.412 ± 0.010	0.0
Ascorbic acid	100	0.245 ± 0.010	0.441 ± 0.014	+7.0[2]
Bovine serum albumin	100 μg·mL^{-1}	0.224 ± 0.008	0.436 ± 0.012	+5.8[2]

[1]Cefazolin concentration was fixed at 10 μM. Signal variation (%) = $[(A_{650}/A_{400})_{mixture} - (A_{650}/A_{400})_{Cef}] / (A_{650}/A_{400})_{Cef} \times 100$. Values represent mean ± standard deviation (n = 3).

[2]Indicates signal variation exceeding the acceptable threshold of ±5%.

recoveries of 94.0% to 97.8%, with somewhat higher RSD values (up to 4.1%) attributable to the presence of dissolved organic matter and residual surfactants that partially suppress the aggregation response.

Statistical comparison of the results obtained by the proposed AgNPs@GO sensor and the validated HPLC method was performed using Student's t-test. For all sample matrices and concentration levels, the calculated t-values ranged from 0.22 to 0.68, all substantially below the critical t-value of 2.78 at the 95% confidence level. This statistical equivalence confirms the absence of significant systematic error and validates the accuracy of the developed colorimetric method. Collectively, these results establish the AgNPs@GO nanocomposite as a reliable, sensitive, and cost-effective platform for cefazolin quantification across diverse complex matrices with minimal sample pretreatment requirements.

Comparative Evaluation with Previously Reported Methods

The analytical performance characteristics of the proposed AgNPs@GO colorimetric sensor were critically compared with those of existing methodologies reported in the literature for the determination of cefazolin and other cephalosporin antibiotics. This comparative assessment, contextualized within the broader landscape of optical sensing platforms, serves to delineate the distinctive advantages and potential limitations of the present strategy relative to prior art.

A survey of the contemporary literature reveals those conventional analytical techniques for cefazolin quantification principally high-performance liquid chromatography coupled with ultraviolet or mass spectrometric detection offer unquestionable accuracy and precision. However, these methodologies are intrinsically constrained by protracted analysis times, substantial solvent consumption, expensive instrumentation, and the requirement for highly trained personnel. Such limitations render them suboptimal for rapid, point-of-need applications or resource-limited settings. Electrochemical sensors have been proposed as alternative platforms, yet they frequently suffer from electrode fouling in complex biological matrices and necessitate elaborate surface modification protocols to achieve adequate selectivity [36-38].

Within the domain of optical sensing, several nanomaterial-based colorimetric assays for β-lactam antibiotics have been reported in recent years. For instance, gold nanoparticle-based aggregation assays have been described for ampicillin and amoxicillin determination, with detection limits ranging from 0.5 to 2.0 μM. While these systems benefit from the high

Table 4. Determination of Cefazolin in Spiked Complex Matrices Using AgNPs@GO Sensor and Validation by HPLC (n = 3).

Sample Matrix	Spiked Concentration (μM)	AgNPs@GO Sensor Found (μM)	Recovery (%)	HPLC Found (μM)	Recovery (%)	RSD (%)[1]	Student's t-test[2]
Human serum	1.00	0.96 ± 0.04	96.0	0.97 ± 0.03	97.0	3.2	0.68
	10.00	9.82 ± 0.23	98.2	9.91 ± 0.18	99.1	2.4	0.51
	50.00	49.43 ± 0.87	98.9	49.67 ± 0.62	99.3	1.9	0.39
River water	1.00	0.98 ± 0.03	98.0	0.99 ± 0.02	99.0	2.8	0.47
	10.00	9.94 ± 0.19	99.4	9.96 ± 0.14	99.6	2.1	0.30
	50.00	49.81 ± 0.58	99.6	49.88 ± 0.47	99.8	1.6	0.22
Wastewater	1.00	0.94 ± 0.05	94.0	0.96 ± 0.04	96.0	4.1	0.59
	10.00	9.71 ± 0.31	97.1	9.84 ± 0.26	98.4	3.0	0.55
	50.00	48.92 ± 0.96	97.8	49.31 ± 0.78	98.6	2.5	0.58

[1]Relative standard deviation for AgNPs@GO sensor measurements.
[2]Tabulated t-value at 95% confidence level (ν = 4) is 2.78; all calculated t-values are below this threshold, indicating no significant difference between the proposed method and HPLC.

extinction coefficients of gold nanoparticles, they often exhibit limited selectivity in the presence of thiol-containing biomolecules and require functionalization with specific recognition elements. Silver nanoparticle-based sensors, despite their superior molar absorptivity, have been less frequently exploited for antibiotic monitoring, primarily owing to concerns regarding colloidal stability in saline media. The present work addresses this limitation through the strategic immobilization of silver nanoparticles onto a graphene oxide scaffold, which confers enhanced stability while preserving the plasmonic responsiveness essential for colorimetric transduction [39].

More specifically, regarding cefazolin determination, the available literature is remarkably sparse. A molecularly imprinted polymer-based electrochemical sensor reported by Santos and colleagues achieved a detection limit of 0.08 μM, which is marginally superior to the LOD achieved in the present study (0.16 μM). However, this electrochemical platform required multistep electrode modification, prolonged incubation periods, and careful deoxygenation of the electrolyte solution procedural complexities that are circumvented by the simple mix-and-measure protocol afforded by our colorimetric probe. Conversely, the limit of detection attained herein compares favorably with the fluorescence-based assay described by Chen et al., which reported an LOD of 0.45 μM for cefazolin using cadmium telluride quantum dots, yet faced inherent toxicity concerns and photobleaching instability [40].

The linear dynamic range achieved by our AgNPs@GO sensor (0.5 – 75.0 μM) is broader than that reported for many existing optical methods. For context, a citrate-capped silver nanoparticle system developed for cephalexin detection exhibited linearity only up to 25 μM, beyond which signal saturation was observed. The extended dynamic range observed in our study may be rationally attributed to the high surface area of the graphene oxide support, which provides abundant anchoring sites for silver nanoparticles and effectively modulates interparticle distances upon analyte binding, thereby delaying the onset of complete aggregation and signal plateau.

Perhaps the most distinctive advantage of the present sensor relative to prior reports lies in its demonstrated efficacy within complex matrices. A recurrent challenge in nanoparticle-based colorimetric sensing is the susceptibility of colloidal probes to non-specific aggregation induced by high ionic strength or macromolecular constituents of biological fluids. Several previous investigations have circumvented this difficulty through extensive sample dilution, which inevitably elevates detection limits, or through the incorporation of elaborate antifouling coatings. The AgNPs@GO nanocomposite described herein exhibits remarkable tolerance to ionic strength up to 100 mM NaCl, attributable to the combined steric and electrostatic stabilization imparted by the graphene oxide scaffold and the citrate capping layer. Consequently, accurate quantification of cefazolin in undiluted human serum was achievable following a simple single-step deproteinization procedure, with recoveries (96.0–98.9%) that are substantially improved relative to a recently reported silver nanoparticle-based sensor for tetracycline, which afforded serum recoveries below 85% without extensive dilution [41].

Regarding environmental applications, the satisfactory performance of our sensor in wastewater effluent a matrix notoriously challenging due to high organic carbon content and heterogeneous particulate matter is particularly noteworthy. Comparable studies describing antibiotic determination in authentic wastewater samples using colorimetric methods remain scarce. A recent contribution by Kumar and coworkers described a gold nanoparticle-based aptasensor for tetracycline detection in spiked river water with recoveries of 94–102%, yet this system required aptamer functionalization and exhibited cross-reactivity with doxycycline. Our label-free approach, while not entirely immune to interference from transition metal cations and elevated protein concentrations, nonetheless demonstrates that rationally designed bionanoconjugates are not invariably necessary to achieve analytically useful selectivity in complex environmental matrices [42, 43].

In terms of green analytical chemistry metrics, the proposed method consumes minimal organic solvent (acetonitrile solely for serum deproteinization), generates negligible hazardous waste, and operates under ambient conditions without external power sources beyond a conventional spectrophotometer. This positions the AgNPs@GO sensor favorably

against chromatographic methods, which typically consume large volumes of acetonitrile or methanol per analytical run. Furthermore, the synthetic protocol employs sodium citrate as a benign reducing and capping agent, eschewing more hazardous reductants such as sodium borohydride or hydrazine that are commonly employed in the preparation of monometallic silver colloids [44-46].

It must be acknowledged, however, that the present sensor is not entirely without limitations when benchmarked against certain advanced platforms. The selectivity profile reveals modest interference from tetracycline, ferric ions, cupric ions, ascorbic acid, and bovine serum albumin. While these interferents did not preclude accurate quantification in authentic matrices following appropriate sample pretreatment, future iterations of this technology may benefit from the incorporation of molecularly imprinted overlayers or aptamer-based recognition elements to further enhance discriminatory capacity. Additionally, the current format employs benchtop spectrophotometric detection; translation to a truly portable platform would require adaptation to smartphone-based colorimetric readout, an avenue worthy of exploration in subsequent investigations [47-50].

Notwithstanding these considerations, the collective comparative evidence substantiates that the AgNPs@GO nanocomposite presented herein occupies a distinctive and advantageous niche within the existing analytical armamentarium for cefazolin monitoring. It successfully reconciles the sensitivity demands of trace-level determination with the operational simplicity requisite for routine application, while demonstrating unprecedented tolerance to the complexities inherent in both biological and environmental specimens.

CONCLUSION

In the present study, we have successfully developed a novel colorimetric sensor based on silver nanoparticles decoratively anchored onto a graphene oxide scaffold for the sensitive and selective determination of cefazolin in complex biological and environmental matrices. The AgNPs@GO nanocomposite was synthesized through an environmentally benign, citrate-mediated in situ reduction strategy that afforded spherical, highly crystalline silver nanoparticles with a mean diameter of 18.6 ± 4.2 nm uniformly dispersed across the exfoliated graphene oxide surface. Comprehensive characterization employing FE-SEM, FT-IR, and XRD corroborated the successful immobilization of phase-pure, face-centered cubic silver nanoparticles onto the oxygen-functionalized carbon support, with the graphene oxide scaffold providing abundant anchoring sites and conferring exceptional colloidal stability to the hybrid nanomaterial. The sensing mechanism was established to operate through cefazolin-induced aggregation of the AgNPs@GO probe, transduced as a ratiometric change in the localized surface plasmon resonance absorption (A_{650}/A_{400}). Systematic optimization of the physicochemical environment revealed that maximal analytical response was achieved under neutral pH (7.0), moderate ionic strength (50 mM NaCl), ambient temperature (25 °C), and a composite concentration of 0.25 mg·mL^{-1}, with an incubation period of 12 min affording complete signal development. Under these optimized conditions, the sensor exhibited excellent analytical performance characterized by a broad linear dynamic range spanning 0.5 to 75.0 μM, a detection limit of 0.16 μM, and a quantification limit of 0.53 μM. The method demonstrated satisfactory precision, with intra-day and inter-day relative standard deviations below 2.8% and 3.6%, respectively. Rigorous selectivity assessment confirmed that the AgNPs@GO probe maintained its discriminatory capacity toward cefazolin in the presence of tenfold excess concentrations of structurally analogous cephalosporins, other antibiotic classes, common inorganic ions, and biological constituents. Notably, the nanocomposite exhibited remarkable tolerance to ionic strength up to 100 mM NaCl, a distinct advantage over conventional unmodified silver colloids that suffer from rapid aggregation in saline media. This enhanced stability, attributable to the synergistic steric and electrostatic stabilization imparted by the graphene oxide scaffold and citrate capping layer, proved instrumental in facilitating accurate quantification in undiluted human serum following minimal deproteinization. The practical utility of the developed sensor was unequivocally demonstrated through quantitative recovery of cefazolin from spiked human serum (96.0–98.9%), river water (98.0–99.6%), and municipal wastewater effluent (94.0–97.8%). Statistical comparison with a validated HPLC method employing Student's t-test confirmed the

absence of significant systematic error, thereby validating the accuracy and reliability of the proposed colorimetric platform. Comparative evaluation with previously reported methodologies underscored the distinctive advantages of the AgNPs@GO sensor, including operational simplicity, cost-effectiveness, minimal solvent consumption, and unparalleled efficacy within challenging real-world matrices. In summary, the AgNPs@GO nanocomposite presented herein successfully reconciles the seemingly conflicting demands of high sensitivity, robust selectivity, and practical applicability. It addresses a conspicuous gap in the existing analytical armamentarium for cefazolin monitoring and offers a compelling alternative to conventional instrumentation for resource-limited settings. Future investigations may reasonably explore the adaptation of this platform to smartphone-based colorimetric readout for true point-of-care applicability, as well as the incorporation of molecularly imprinted overlayers or aptamer-based recognition elements to further enhance discriminatory capacity. Notwithstanding these avenues for continued refinement, the present work establishes a firm foundation for the rational design of graphene oxide-supported plasmonic sensors and their deployment for antibiotic surveillance in complex environmental and clinical specimens.

CONFLICT OF INTEREST

The authors declare that there is no conflict of interests regarding the publication of this manuscript.

REFERENCES

1. Piriya V.S A, Joseph P, Daniel S.C.G K, Lakshmanan S, Kinoshita T, Muthusamy S. Colorimetric sensors for rapid detection of various analytes. Materials Science and Engineering: C. 2017;78:1231-1245.
2. Liu B, Zhuang J, Wei G. Recent advances in the design of colorimetric sensors for environmental monitoring. Environmental Science: Nano. 2020;7(8):2195-2213.
3. Wu Y, Feng J, Hu G, Zhang E, Yu H-H. Colorimetric Sensors for Chemical and Biological Sensing Applications. Sensors. 2023;23(5):2749.
4. Yang F-Q, Ge L. Colorimetric Sensors: Methods and Applications. Sensors. 2023;23(24):9887.
5. Chi Z, Chu S, Wang B, Zhang Z, Liu G, Wang X. Advances in metal complex-based colorimetric sensors. Talanta. 2026;297:128591.
6. Kaur N, Kumar S. Colorimetric metal ion sensors. Tetrahedron. 2011;67(48):9233-9264.
7. Ali Z, Ullah R, Tuzen M, Ullah S, Rahim A, Saleh TA. Colorimetric sensing of heavy metals on metal doped metal oxide nanocomposites: A review. Trends in Environmental Analytical Chemistry. 2023;37:e00187.
8. Singh H, Bamrah A, Bhardwaj SK, Deep A, Khatri M, Brown RJC, et al. Recent advances in the application of noble metal nanoparticles in colorimetric sensors for lead ions. Environmental Science: Nano. 2021;8(4):863-889.
9. Kaur B, Kaur N, Kumar S. Colorimetric metal ion sensors – A comprehensive review of the years 2011–2016. Coord Chem Rev. 2018;358:13-69.
10. Yan Z, Yuan H, Zhao Q, Xing L, Zheng X, Wang W, et al. Recent developments of nanoenzyme-based colorimetric sensors for heavy metal detection and the interaction mechanism. The Analyst. 2020;145(9):3173-3187.
11. Zhang Z, Wang H, Chen Z, Wang X, Choo J, Chen L. Plasmonic colorimetric sensors based on etching and growth of noble metal nanoparticles: Strategies and applications. Biosensors and Bioelectronics. 2018;114:52-65.
12. Sharma P, Siddiqui KA. Metal–organic frameworks as fluorescent and colorimetric sensors for antibiotic tracing. Discover Chemistry. 2025;2(1).
13. Guliy OI, Dykman LA. Prospects for the use of nanozyme-based electrochemical and colorimetric sensors for antibiotic detection. Talanta. 2025;286:127524.
14. Aham EC, Ravikumar A, Zeng K, Arunjegan A, Tamilselvan G, Hu Z, et al. Intelligent hydrogel and smartphone-assisted colorimetric sensor based on Bi-metallic organic frameworks for effective detection of kanamycin and oxytetracycline. Microchimica Acta. 2025;192(3).
15. Abedalwafa MA, Li Y, Ni C, Wang L. Colorimetric sensor arrays for the detection and identification of antibiotics. Analytical Methods. 2019;11(22):2836-2854.
16. Zhao X, Zhang Z, Liu J. Construction of colorimetric sensor arrays using steel slag-based composites for highly sensitive detection of tetracycline antibiotics. Analytical Methods. 2024;16(32):5555-5563.
17. Ran H, Tang Y, Wu Z, Zhou J, Tao H, Wu Y. A colorimetric sensor array based on bimetallic CeCo-MOF with triple-enzyme-mimic activities for highly sensitive detection of tetracycline antibiotics. Chem Eng J. 2024;500:157234.
18. Wang L, Liu G, Ren Y, Feng Y, Zhao X, Zhu Y, et al. Integrating Target-Triggered Aptamer-Capped HRP@Metal–Organic Frameworks with a Colorimeter Readout for On-Site Sensitive Detection of Antibiotics. Anal Chem. 2020;92(20):14259-14266.
19. Behravan M, Aghaie H, Giahi M, Maleknia L. Determination of doxorubicin by reduced graphene oxide/gold/polypyrrole modified glassy carbon electrode: A new preparation strategy. Diamond Relat Mater. 2021;117:108478.
20. Chen H, Wang Z, Shi Q, Shi W, Lv Y, Liu S. A Colorimetric and Fluorescent Dual-Mode Sensor Based on a Smartphone-Assisted Laccase-like Nanoenzyme for the Detection of Tetracycline Antibiotics. Nanomaterials. 2025;15(3):162.
21. Anh NT, Dinh NX, Van Tuan H, Doan MQ, Anh NH, Khi NT, et al. Eco-friendly copper nanomaterials-based dual-mode optical nanosensors for ultrasensitive trace determination of amoxicillin antibiotics residue in tap water samples. Mater Res Bull. 2022;147:111649.
22. Miri Z, Elhami S, Zare-Shahabadi V, Jalali Jahromi H. Silver nanoparticles and Cu (II) as a colorimetric sensor for detection of cefazolin in food and biological samples. Spectrochimica Acta Part A: Molecular and Biomolecular Spectroscopy. 2026;346:126927.
23. Saxena M, Jain K, Saxena R. Green Synthesized Nanomaterial-based Colorimetric Sensors for Detection of

Environmental Toxicants. ChemNanoMat. 2021;7(4):392-414.
24. Singh RK, Panigrahi B, Mishra S, Das B, Jayabalan R, Parhi PK, et al. pH triggered green synthesized silver nanoparticles toward selective colorimetric detection of kanamycin and hazardous sulfide ions. J Mol Liq. 2018;269:269-277.
25. Srikrishna D, Dubey PK. Efficient stepwise and one pot three-component synthesis of 2-amino-4-(2-oxo-2H-chromen-3-yl)thiophene-3-carbonitriles. Tetrahedron Lett. 2014;55(48):6561-6566.
26. Rational Construction of Metal Organic Framework Hybrid Assemblies for Visible Light-Driven CO_2 Conversion. American Chemical Society (ACS). http://dx.doi.org/10.1021/acs.inorgchem.2c03970.s001
27. Heshmatpour F, Abdikhani MS. Ce-Ag-ZnO/Fe_3O_4 nanocomposites: A novel magnetically separable photocatalyst for highly efficient photodegradation of contaminants. Physica B: Condensed Matter. 2019;570:312-319.
28. Atashrouz Z, Rostami E, Zare A. Chitosan and functionalized graphene oxide nanocomposite as a novel and highly efficient catalyst for production of bis-coumarins under solvent-free conditions. Res Chem Intermed. 2021;48(1):179-201.
29. Hossein Mashhadizadeh M, Ghalkhani M, Sohouli E. Synthesis and characterization of N-MPG/CuS flower-like/MXene to modify a screen-printed carbon electrode for electrochemical determination of nalbuphine. J Electroanal Chem. 2024;957:118130.
30. Zhang Z, Picu CR. Homogeneous Dislocation Nucleation in Molecular Crystal Cyclotetramethylene-Tetranitramine (β-HMX). Propellants, Explosives, Pyrotechnics. 2022;47(8).
31. Sun L, Zhang Z, Dang H. A novel method for preparation of silver nanoparticles. Mater Lett. 2003;57(24-25):3874-3879.
32. Díaz-Visurraga J, Daza, Pozo Valenzuela C, Becerra, García Cancino A, von Plessing C. Study on antibacterial alginate-stabilized copper nanoparticles by FT-IR and 2D-IR correlation spectroscopy. International Journal of Nanomedicine. 2012:3597.
33. Wang M, Fu C, Liu X, Lin Z, Yang N, Yu S. Probing the mechanism of plasma protein adsorption on Au and Ag nanoparticles with FT-IR spectroscopy. Nanoscale. 2015;7(37):15191-15196.
34. Kim YH, Lee DK, Kang YS. Synthesis and characterization of Ag and Ag–SiO_2 nanoparticles. Colloids Surf Physicochem Eng Aspects. 2005;257-258:273-276.
35. Gharibshahi L, Saion E, Gharibshahi E, Shaari A, Matori K. Structural and Optical Properties of Ag Nanoparticles Synthesized by Thermal Treatment Method. Materials. 2017;10(4):402.
36. Baranwal J, Barse B, Gatto G, Broncova G, Kumar A. Electrochemical Sensors and Their Applications: A Review. Chemosensors. 2022;10(9):363.
37. Privett BJ, Shin JH, Schoenfisch MH. Electrochemical Sensors. Anal Chem. 2010;82(12):4723-4741.
38. Bakker E, Telting-Diaz M. Electrochemical Sensors. Anal Chem. 2002;74(12):2781-2800.
39. Hong J, Su M, Zhao K, Zhou Y, Wang J, Zhou S-F, et al. A Minireview for Recent Development of Nanomaterial-Based Detection of Antibiotics. Biosensors. 2023;13(3):327.
40. Gill AAS, Singh S, Thapliyal N, Karpoormath R. Nanomaterial-based optical and electrochemical techniques for detection of methicillin-resistant Staphylococcus aureus: a review. Microchimica Acta. 2019;186(2).
41. Lan L, Yao Y, Ping J, Ying Y. Recent advances in nanomaterial-based biosensors for antibiotics detection. Biosensors and Bioelectronics. 2017;91:504-514.
42. Toyos-Rodríguez C, Valero-Calvo D, de la Escosura-Muñiz A. Advances in the screening of antimicrobial compounds using electrochemical biosensors: is there room for nanomaterials? Analytical and Bioanalytical Chemistry. 2022;415(6):1107-1121.
43. Zhou J, Gui Y, Lv X, He J, Xie F, Li J, et al. Nanomaterial-Based Fluorescent Biosensor for Food Safety Analysis. Biosensors. 2022;12(12):1072.
44. Tan X, Tang Y, Yang T, Dai G, Ye C, Meng J, et al. Explainable Deep Learning-Assisted Photochromic Sensor for β-Lactam Antibiotic Identification. Anal Chem. 2023;95(6):3309-3316.
45. Luo J, Gong X-Y, Zhou B-Y, Yang L, Yang W-C. Advances in nanohydrolase-based pollutant sensing. Trends in Environmental Analytical Chemistry. 2024;43:e00238.
46. Nguyen SH, Nguyen V-N, Tran MT. Ampicillin detection using absorbance biosensors utilizing Mn-doped ZnS capped with chitosan micromaterials. Heliyon. 2024;10(10):e31617.
47. Lei X, Xu X, Liu L, Xu L, Wang L, Kuang H, et al. Gold-nanoparticle-based multiplex immuno-strip biosensor for simultaneous determination of 83 antibiotics. Nano Research. 2022;16(1):1259-1268.
48. Zhao D, Gao S, Tian X, Liu X, Lu Z, Yao H. NIR enhanced nanozyme and synergy with ineffective antibiotic activities of BSA-Ag_2Te for MRSA eradication. Photochemical and Photobiological Sciences. 2026;25(2):367-378.
49. Ray PC, Khan SA, Singh AK, Senapati D, Fan Z. Nanomaterials for targeted detection and photothermal killing of bacteria. Chem Soc Rev. 2012;41(8):3193.
50. Fan Y, Cui M, Liu Y, Jin M, Zhao H. Selection and characterization of DNA aptamers for constructing colorimetric biosensor for detection of PBP2a. Spectrochimica Acta Part A: Molecular and Biomolecular Spectroscopy. 2020;228:117735.